Physica B 480 (2016) 42–47

Contents lists available at ScienceDirect

Physica B

journal homepage: www.elsevier.com/locate/physb

Surface characterization of ZnO nanorods grown by chemical bath deposition

C.M. Mbulanga [a,*], Z.N. Urgessa [a], S.R. Tankio Djiokap [a], J.R. Botha [a], M.M. Duvenhage [b], H.C. Swart [b]

[a] Department of Physics, Nelson Mandela Metropolitan University, P.O. Box 77000, Port Elizabeth 6031, South Africa
[b] Department of Physics, University of the Free State, P.O Box 77000, Bloemfontein ZA9300, South Africa

ARTICLE INFO

Article history:
Received 13 May 2015
Received in revised form
15 July 2015
Accepted 16 July 2015
Available online 7 August 2015

Keywords:
Zinc oxide (ZnO)
Chemical bath deposition (CBD)
Time-of-Flight Secondary Ion Mass Spectroscopy (TOF-SIMS)
X-ray Photoelectron Spectroscopy (XPS)
Auger Electron Spectroscopy (AES)
Hydrogen diffusion

ABSTRACT

The surface composition of as-grown and annealed ZnO nanorods (ZNs) grown by a two-step chemical bath deposition method is investigated by the following surface-sensitive techniques: Time-of-Flight Secondary Ion Mass Spectroscopy (TOF-SIMS), X-ray Photoelectron Spectroscopy (XPS) and Auger Electron Spectroscopy (AES). The presence of H on the surface and throughout the entire thickness of ZNs is confirmed by TOF-SIMS. Based on TOF-SIMS results, the O2 XPS peak mostly observable at ~531.5 is assigned to O bound to H. Furthermore, it is found that the near surface region of as-grown ZNs is Zn-rich, and annealing at high temperature (~850 °C) removes H-related defects from the surface of ZNs and affect the balance of zinc and oxygen concentrations.

© 2015 Elsevier B.V. All rights reserved.

1. Introduction

Zinc oxide (ZnO) with its interesting properties, such as a large direct band gap and stable exciton even above room temperature (binding energy of 60 meV), has gained substantial interest in the research community [1–7]. Specifically, a growing interest exists in quasi-one-dimensional ZnO nanostructures (e.g. nanorods, nanowires, nanobelts and nanotubes), considered as potential candidates for applications such as gas sensors [1], biosensors [2–3], nanolasers [4], optical waveguides [5–6], and light emitting diodes [4,7]. However, nanostructured materials have a large surface-to-volume ratio compared to epilayer material, which amplifies surface related effects in many ways [1–7]. For optoelectronic applications such as light emitting diodes and solar cells, surface states in the band gap can lead to technical challenges. These states are mostly due to non-stoichiometry, adsorbed foreign species and intrinsic defects in the near-surface region of ZnO. For example, the incorporation of H in ZnO has been shown by cathodoluminescence spectroscopy to strongly affect the green luminescence in ZnO, and indeed in different ways, depending on deviations from the ideal stoichiometry [8]. Bai et al. [9] reported also that the high surface coverage by the OH-group can affect strongly the sensitivity of ZnO sensors. Yang et al. [10], based on XPS investigations, showed a correlation between surface recombination and the presence of OH-bonds and chemisorbed oxygen on the surface of solution-grown ZnO nanorod arrays, as well as H-bonds on $(000\bar{1})$ surfaces. Therefore, it is important to investigate the complete chemical composition and distribution of impurities in ZnO, the surface stoichiometry and to identify the chemical origin and nature of surface recombination centers in ZnO nanostructures [11–16].

In this work, we report surface-sensitive experimental results for solution-grown ZnO nanorods (ZNs). On the one hand, the chemical composition as function of depth was studied by Time-of-Flight Secondary Ion Mass Spectroscopy (TOF-SIMS). On the other hand, X-ray Photoelectron Spectroscopy (XPS) and Auger Electron Spectroscopy (AES) were used to investigate the stoichiometry of the ZnO nanorod surfaces as function of annealing temperature.

2. Experimental details

The ZNs used in this investigation were grown on Si substrate by chemical bath deposition (CBD) as reported recently by Urgessa

* Corresponding author.
E-mail address: crispin.mbulanga@nmmu.ac.za (C.M. Mbulanga).

http://dx.doi.org/10.1016/j.physb.2015.07.016
0921-4526/© 2015 Elsevier B.V. All rights reserved.

et al. [14]. Two steps were followed: firstly the deposition of a ZnO seed layer on a cleaned silicon substrate (001), and secondly the growth of ZNs on the pre-treated substrate at 85 °C in an aqueous mixture of zinc nitrate hexahydrate and hexamine (pH 5.5). Before the deposition of the seed layer, the substrate was cleaned sequentially using trichloroethylene (TCE), acetone, methanol, and de-ionized (DI) water and blown dry in nitrogen gas. A well agitated ethanolic solution made of 5 mM of zinc acetate dihydrate ($Zn(CH_3COO)_2 \cdot 2H_2O$) and 0.0101 g of polyvinylpyrrolidone (PVP) was spun five times onto the pre-cleaned substrate using a spin coater. Then the spin coated substrate was annealed in an oxygen environment for 30 min at 300 °C at atmospheric pressure. This spin coating and annealing process was repeated twice. For the formation of the nanorods, the seeded substrate was immersed into the growth solution, which was a mixture of aqueous solutions of zinc nitrate hexahydrate ($Zn(NO_3 \cdot 6H_2O)$) and hexamethylenetetramine (hexamine) ($C_6H_{12}N_4$). After growth, ZN samples were cleaned with deionised water and blown dry by nitrogen gas. For further treatment and different investigations, the dried sample was cleaved into several pieces and kept in clean non-sealed containers. Annealing experiments were conducted in a horizontal quartz tube at 300 °C, 400 °C, 500 °C, 600 °C and 850 °C in controlled flows of N_2 and O_2 for 30 min.

A field emission scanning electron microscope (SEM) (JEOL 7001F FESEM) was used to investigate the morphologies of the nanostructures. The crystalline nature of the nanostructures was confirmed using a Bruker D8 Discover X-ray Diffractometer with a Cu-Kα X-ray source ($\lambda = 1.5405$ Å). A detailed description of the TOF-SIMS system is given elsewhere [15]. It is worth noting that depth profile investigations were done in ultra-high vacuum of $\sim 10^{-8}$ mbar for positive ion spectroscopy and $\sim 10^{-9}$ mbar for negative ion spectroscopy. Only an area of $100 \times 100\ \mu m^2$ was analyzed from a $300 \times 300\ \mu m^2$ sputtered area, in order to avoid edge effects. Sputtering was done in the positive mode by an oxygen gun (1 keV, 250 nA) and in the negative mode by a cesium gun (2 keV, 130 nA). Detailed surface analysis was done by a PHI 5000 Versaprobe-Scanning ESCA Microprobe (XPS) [17] and a PHI 700 Scanning Auger Nanoprobe. The excitation beam for XPS and AES measurements was ~100 μm and ~10 nm in diameter, respectively. Sputtering during XPS and AES experiments was performed with an Ar ion gun at a rate of ~18 nm/min and ~22 nm/min, respectively. The energy resolution of both systems is 0.5 eV and the margin for error of the detector of photoelectrons and Auger electrons, are 2% and 5%, respectively. XPS and AES experiments were done at 4×10^{-9} Torr and 2.85×10^{-10} Torr, respectively.

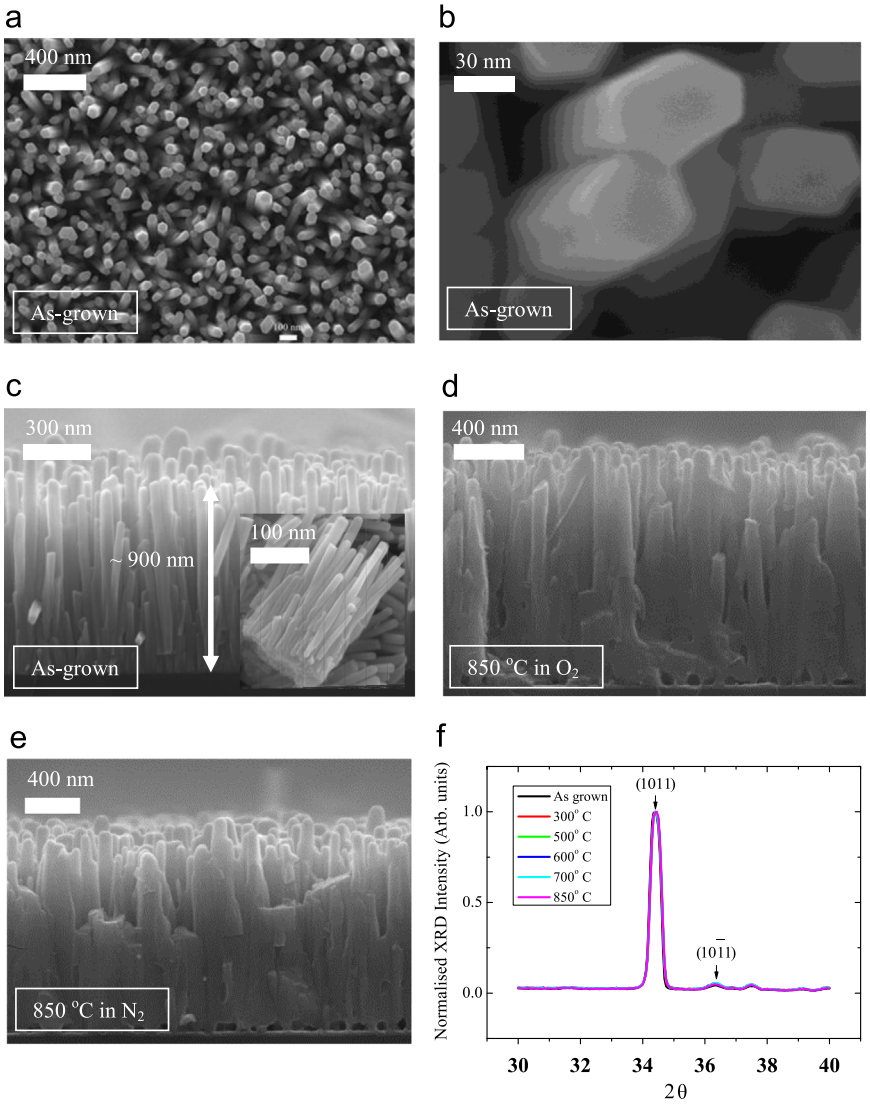

Fig. 1. (a–c) Typical top view and cross sectional SEM micrographs of the as-grown ZNs. (d, e) Typical cross sectional SEM micrograph of ZNs annealed at 850 °C for 30 min respectively in O_2 and N_2. (f) Normalized XRD spectra of as-grown ZNs and oxygen-annealed samples.

3. Results

3.1. Structure and morphology of ZnO nanorods

Fig. 1a–c shows respectively typical top view and cross sectional SEM micrographs of as-grown ZNs. The insets in Fig. 1c show a bunch of as-grown ZNs broken off from the substrate during cleaving. Fig. 1d and e shows typical cross sectional SEM micrographs of ZNs annealed at 850 °C in O_2 and N_2, respectively. Fig. 1f presents normalized XRD spectra of as-grown and oxygen-annealed ZNs. XRD investigations of ZNs annealed in N_2 are not reported here due to the similar behavior compared to ZNs annealed in O_2. It can be seen from Fig. 1a and b that ZNs are uniformly distributed on the substrate and exhibit a hexagonal cross-section. The average diameter estimated from SEM micrographs is ~45 nm. As can be seen from Fig. 1c, despite the fact that ZNs are approximately perpendicular to the substrate, they are also attached to one another at their base (see inset) and are more sparsely spaced towards the top of the sample, having an average length of ~900 nm. Fig. 1d and e illustrates similar morphological changes after annealing at 850 °C, irrespective of the environment. In particular, voids can be seen at the interface with the substrate. Although the melting point of ZnO is 1975 °C, the rods appear to have "melted" into one another. The large voids at the interface may be due to vacancy formation and migration, as well as a form of Ostwald ripening. Furthermore, Fig. 1f shows that, irrespective of annealing temperature, a strong diffraction at 34.4° 2θ from the (0002) plane of wurtzite ZnO is observed in all cases. As there is not any significant shift in the peak position of the (0002) peak, the d_{0002} spacing between adjacent (0002) lattice planes is found to be unaffected by annealing. Hence the SEM and XRD experimental results show that under the specified annealing conditions, the orientation of the ZNs does not change.

3.2. TOF-SIMS, XPS and AES analysis of ZnO nanorods

TOF-SIMS results of ZNs are shown in Figs. 2 and 3. Fig. 2a–f illustrates the chemical elements present in ZNs as function of depth. However, at this point it should be pointed out that depth profiles were recorded as function of sputter time, which is

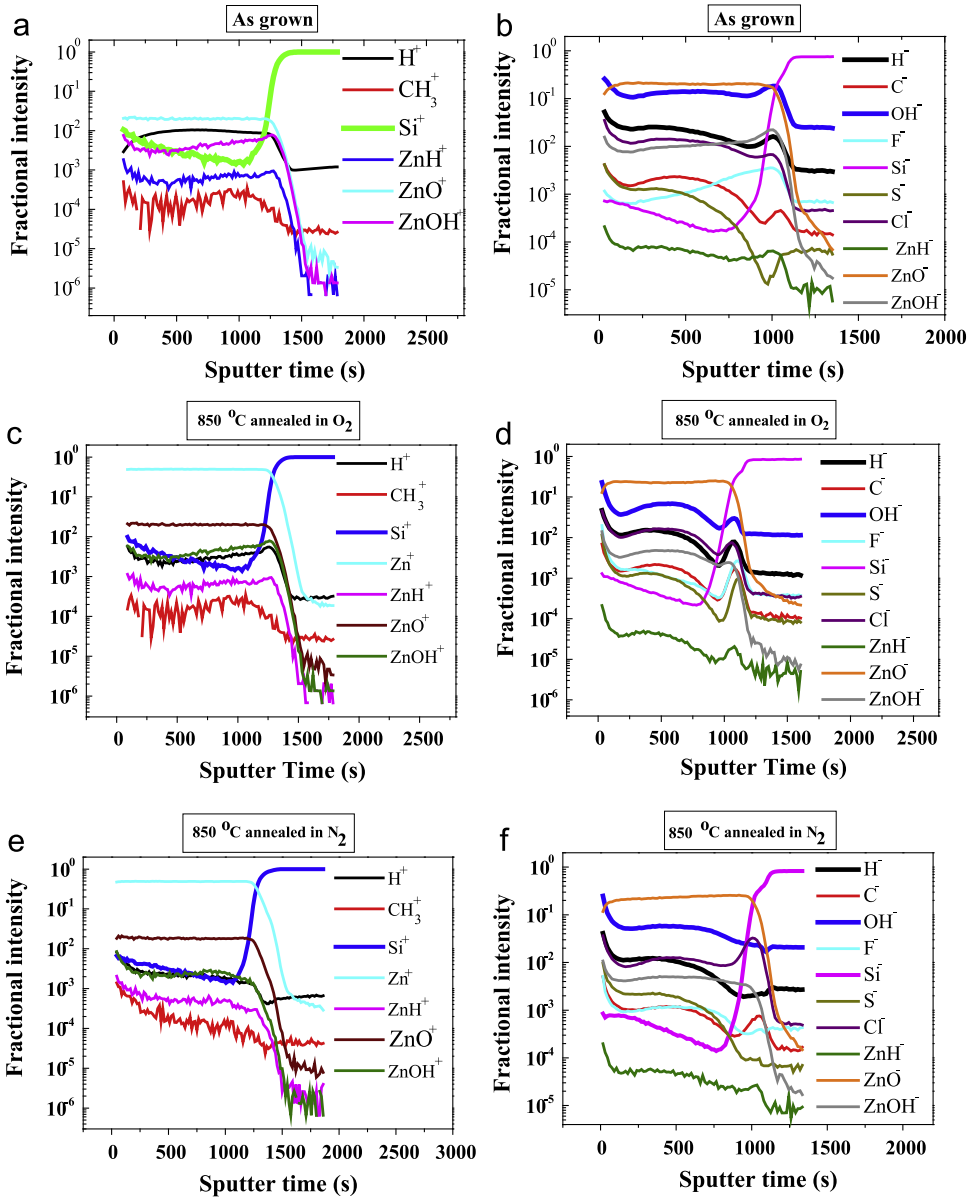

Fig. 2. TOF-SIMS depth profiles of positive ions (a, c, e) and negative ions (b, d, f) from as-grown and annealed ZNs.

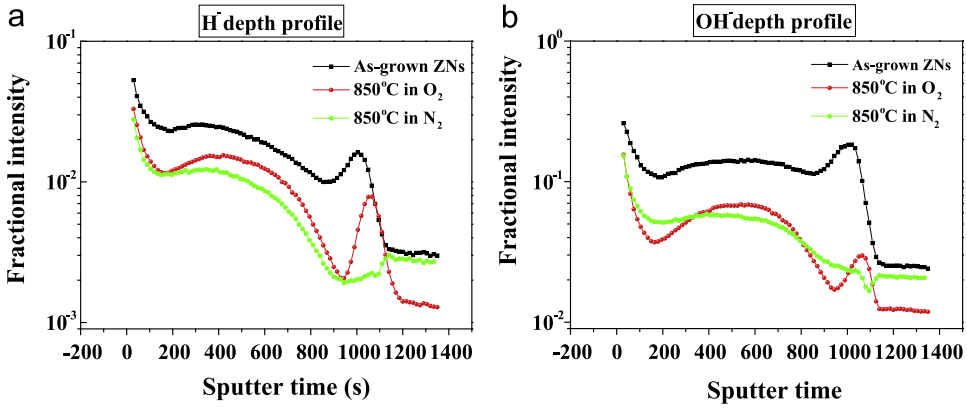

Fig. 3. TOF-SIMS depth profiles of (a) H^- and (b) OH^- species in as-grown ZNs and ZNs annealed at 850 °C in O_2 and in N_2, respectively.

defined as the number of scans times the sputter interval. In this experiment the sputter interval was 15 s. Fig. 2a, c and e presents depth profiles of positive secondary ions, whereas Fig. 2b, d and f shows profiles of negative secondary ions.

From Fig. 2a, it can be seen that as-grown ZNs contain H^+, CH_3^+, ZnO^+, ZnH^+ and $ZnOH^+$ species. The hydrocarbons were probably adsorbed on the nanorods from the ambient environment. However, the H^+, ZnH^+ and $ZnOH^+$ species most likely originate from hydrogen and hydroxyl groups incorporated into the crystals during growth from solution. Fig. 2b illustrates that in addition to these species F^-, S^-, and Cl^- are also present in the samples. The C^- signal probably stems from the hydrocarbons seen in Fig. 2a, while Cl and S will have been incorporated during growth, since the zinc nitrate hexahydrate ($Zn(NO_3 \cdot 6H_2O)$) and hexamethylenetetramine (hexamine) ($C_6H_{12}N_4$) used as precursors contained ≤ 50 mg/kg of Cl and ≤ 100 mg/kg of sulfate. However, the origin of F is unknown. The same elements have been observed also in samples annealed at 850 °C in N_2 and O_2, respectively, as shown in Fig. 2d and f.

An accumulation of H^-, OH^-, $ZnH^{-/+}$, and $ZnOH^{-/+}$ species is observable in the near-surface region of the sample, as well as near the substrate interface. The latter effect is observed more clearly in negative spectroscopy.

Depth profiles of H^- and OH^- in as grown and 850 °C-annealed ZNs are compared in Fig. 3a and b, respectively, in order to illustrate the effect of annealing on the distributions of these impurities. The following observations can be made: (i) the H^- and OH^- signals increase in the "near surface region" of the as-grown samples; (ii) these signals decrease after annealing, but are still observed from the "bulk" of the films; (iii) the accumulation of hydrogen near the substrate interface reduces after annealing in nitrogen only.

Results from XPS and AES are summarized in Figs. 4 and 5. Fig. 4a presents the O 1s XPS signal from the as-grown ZNs, while Fig. 4b presents O 1s XPS signal in ZNs annealed at 850 °C in N_2. (Note that XPS provides information about the first 1–2 nm from the surface.) Two distinct peaks centered around 530.0 ± 0.35 eV and 531.5 ± 0.35 eV, commonly called O1 and O2, respectively, are distinguished. The full-widths at half-maximum (FWHM) are 1.1 eV and 1.5 eV, respectively. The O1 peak is associated with O^{2-} ions in the wurtzite structure, surrounded by four Zn^{2+} ions with their full complement of nearest-neighbor O^{2-} ions [17–18]. Based on the TOF-SIMS results, the peak O2 is assigned to O bound to H. Similar assignments have been made for the XPS signals from ZnO nanoflowers [19] and nanorods [10,19]. The removal of ~9 nm by sputtering did not significantly affect the relative intensities of the O1 and O2 peaks in each case (see Fig. 4a and b). This is ascribed to the specific morphology of the samples: the large variations in surface height resulting from the columnar crystals will leave a substantial surface area unchanged after sputtering. Two symmetric Zn $2p_{1/2}$ and $2p_{3/2}$ XPS peaks, associated with Zn^{2+} ions in the wurtzite structure surrounded by O atoms with their full complement of nearest-neighbors Zn^{2+} ions, were also detected (not shown here) at respectively 1021.3 ± 0.35 eV (Zn $2p_{3/2}$) and 1044.4 ± 0.35 eV.

Finally, Fig. 5 presents the Zn/O-ratios obtained from XPS and AES on as-grown and annealed ZN samples. Only atomic concentrations measured after sputtering were calculated and considered in order to minimize the contributions of impurities to the spectra. Fig. 5a shows the Zn/O-ratios (from XPS) in as-grown ZNs and samples annealed at 850 °C in N_2 and O_2, respectively, while Fig. 5b shows Zn/O-ratios obtained from AES on *cross-sections* of as-grown ZNs and the sample annealed at 850 °C in N_2. It is clear

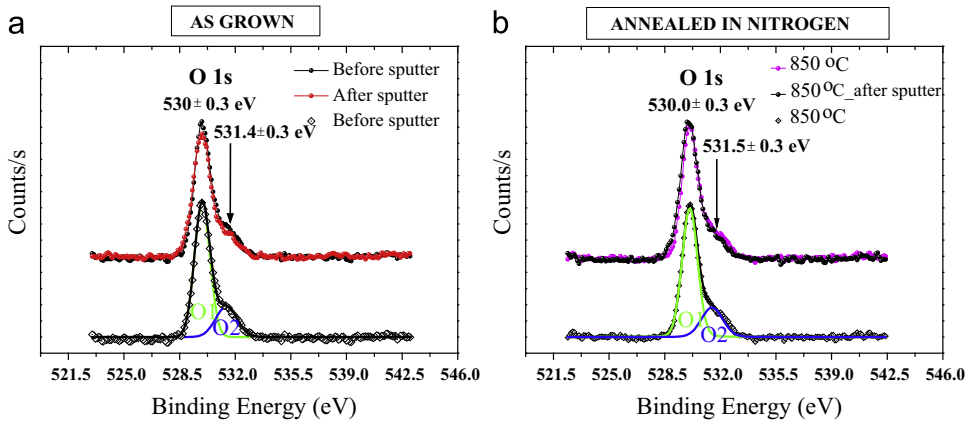

Fig. 4. O 1s core level XPS spectra before and after sputtering from as-grown ZNs (a) and a sample annealed at 850 °C in N_2 (b).

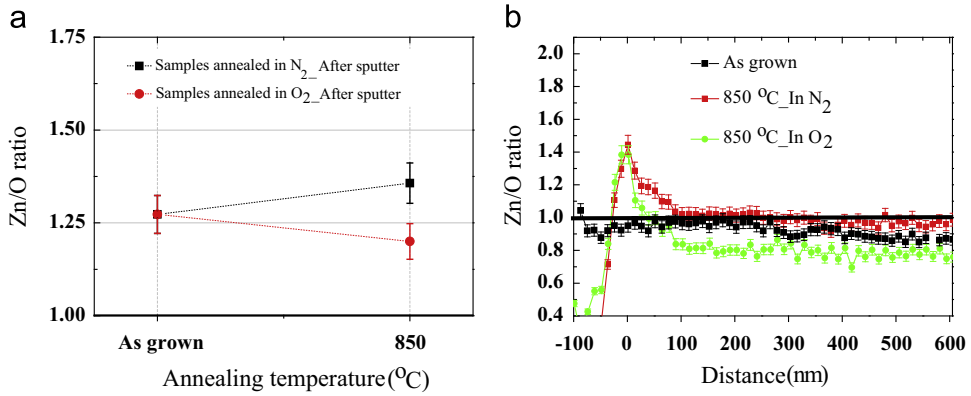

Fig. 5. Zn/O ratios from sputtered ZNs samples, obtained from (a) XPS on the top surface of the samples and (b) AES on cross-sections of the samples.

from Fig. 5a that the Zn/O ratios are above 1, irrespective of annealing environment and temperature. It follows that the analyzed region (up to 2 nm below the surface) is Zn-rich, suggesting that the most abundant intrinsic defects in the near-surface region of as-grown and 850 °C-annealed ZNs are oxygen vacancy-related. The high concentration of Zn cannot be attributed to Zn_i (Zn interstitials) because at room temperature Zn_i diffuse. In fact, Gorelkinskii et al. [20] experimentally observed PL bands related to interstitials created by electron irradiation at 4.2 K in undoped single crystal ZnO quenching as a function of annealing (form 4.2 K to RT) and witnessed their complete disappearance at RT. Furthermore, V_O has a much lower formation energy (1.34 eV) than V_{Zn} (6.94 eV) in ZnO under Zn-rich conditions according to LDA+U calculations [21]. It can be seen in Fig. 5b (obtained from AES on cross-sectional samples) that as-grown ZNs are nearly stoichiometric throughout the sample. Annealing at 850 °C results in the formation of a Zn-rich region, extending to a depth of ~100 nm from the top surface, irrespective of the ambient. In the "bulk" of the samples, annealing in N_2 leaves the ZNs stoichiometric, while annealing in O_2 results in O-rich material.

4. Discussion

The accumulation of hydrogen near the surface of as-grown ZNs has been observed by many research groups. For example, Yang et al., using XPS, deduced the presence of H in the "near surface region" from the O–H-related O 1s peak at 531.5 eV [10]. An excitonic recombination line (I_4) attributed to H in oxygen vacancies (H_O) was observed in the PL of as-grown ZNs in our own laboratory (see [14]), which disappeared after annealing at 450 °C, irrespective of the annealing environment. The drop in the SIMS signals from hydrogen-containing ions in the "the near surface region" and in the bulk of the samples after annealing indeed confirms the out-diffusion of hydrogen species. The observed hydrogen "accumulation" in the "near surface region", even in annealed ZNs is ascribed to adsorption from the ambient (i.e. hydrogen containing species adsorbing to the polar surfaces in the time between annealing and SIMS analysis). As a result of sputtering (to produce the depth profiles) the surface morphology of the samples will change, resulting in an effectively smaller surface area as the sample surface evens out/flattens.

Based on comparisons of time decays of excitons in as-grown and 500 °C-annealed ZNs, Yang et al. [10] suggested the existence of remnant H bound to O (O2) near the surface, even after 1 h of annealing that did not totally anneal out [10]. This may explain the origin of observed accumulation of OH^- species as a combination of those remnant OH species (or O–H bond) from the diffusion process from the bulk region of ZNs and of newly adsorbed OH species (or O–H bond) from the ambient environment. The detection of H-containing ions throughout the entire thickness of the samples, even after annealing at 850 °C in the present work, seemingly contradicts PL data that confirmed a complete out-diffusion of H_O and H_{BC} from bulk ZnO [22] and ZNs [14] after annealing at high temperatures. PL probes the "near surface" of the sample, rather than the "bulk region", and may therefore not be sensitive to hydrogen in the bulk. Furthermore, hydrogen atoms may combine to form molecules upon annealing, which will contribute to the SIMS signals but not to the excitonic PL spectrum for ZnO.

5. Conclusion

In this paper, we performed TOF-SIMS, XPS and AES investigations on as-grown and annealed ZN films. The complete chemical composition and distribution of impurities in ZNs was investigated, as well as the effect of annealing on the surface-related stoichiometry. The presence of H-related species on the top surface and throughout the entire depth of as-grown films was confirmed. The surface of as-grown ZNs (analyzed both from the top and from cross-sections of the films) was found to be Zn-rich. Furthermore, annealing at high temperature (850 °C) reduced the surface hydrogen concentration on ZNs, and affect the balance of zinc and oxygen concentrations. These results will stimulate further research to completely suppress the presence of H-related defects in ZNs and to control the generation of intrinsic defects in ZNs by annealing, which will prompt the practical application of ZNs in the future.

References

[1] H. Zhang, J.B. Wu, C.X. Zhai, N. Du, X.Y. Ma, D.R. Yang, Nanotechnology 18 (2007) 455604.
[2] A. Umar, M.M. Rahman, S.H. Kim, Y.B. Hahn, J. Nanosci. Nanotechnol. 8 (2008) 3216.
[3] S. Al-Hill, M. Willander, Nanotechnology 20 (2009) 175103.
[4] X. Duan, Y. Huang, R. Agarwal, C.M. Lieber, Nature 241 (2003) 421.
[5] A.B. Greytak, C.J. Barrelet, Y. Li, C.M. Lieber, Appl. Phys. Lett. 87 (2005) 151103.
[6] M. Law, D.J. Sirbuly, J.C. Johnson, J. Goldberger, R.J. Saykally, P. Yang, Science 305 (2004) 1269.
[7] J.C. Johnson, H.J. Choi, K.P. Knutsen, R.D. Schaller, P. Yang, R.J. Saykally, Nat. Mater. Chem. 1 (2002) 106.
[8] C. Ton-That, L. Weston, M.R. Philips, Phys. Rev. 86 (2012) 115205.
[9] Z.K. Bai, C.S. Xie, M.L. Hu, S.P. Zhang, D.W. Zeng, Mater. Sci. Eng. B 149 (2008) 12.
[10] L.L. Yang, Q.X. Zhao, M. Willander, X.J. Liu, M. Fahlman, J.H. Yang, Appl. Surf. Sci. 256 (2010) 3592.
[11] Q. Wan., T.H. Wang, J.C. Zhao, Appl. Phys. Lett. 87 (2005) 083105.
[12] S.C. Erwin, L. Zu, M.I. Haftel, A.L. Efros, T.A. Kennedy, D.J. Norris, Nature 436 (2005) 91.
[13] P. Zhang, E. Tevaarwerk, B. Park, D.E. Savage, G.K. Celler, I. Knezevic, P.G. Evans, M.A. Erikkson, M.G. Lagally, Nature 439 (2006) 671.

[14] Z.N. Urgessa, J.R. Botha, M.O. Eriksson, C.M. Mbulanga, S.R. Dobson, S.R. Tankio Djiokap, K.F. Karlsson, V. Khranovskyy, R. Yakimova, Per-Olof Holtz, J. Appl. Phys. 116 (2014) 123506.
[15] A. Yousif, R.M. Jafer, J.J. Terblans, O.M. Ntwaeaborwa, M.M. Duvenhage, Appl. Surf. Sci. 313 (2014) 524.
[16] F.V. Molefe, L.F. Koao, B.F. Dejene, H.C. Swart, Opt. Mater. 46 (2015) 292.
[17] V. Kumar, H.C. Swart, O.M. Ntwaeaborwa, R.E. Kroon, J.J. Terblans, S.K.K. Shaat, A. Yousif, M.M. Duvenhage, Mater. Lett. 101 (2013) 57.
[18] J.F. Moulder, W.F. Stricle, P.E. Sobol, K.D. Bomben, Handbook of X-ray Photoelectron Spectroscopy, ULVAC-PHI, Inc., Chigasaki, 1992.
[19] R. Al-Gaashani, S. Radiman, A.R. Daud, N. Tabet, Y. Al-Douri, Ceram. Int. 39 (2013) 2283.
[20] Y.V. Gorelkinskii, G.D. Watkins, Phys. Rev. B 69 (2004) 115212.
[21] A. Janotti, C.G. Van de Walle, Phys. Rev. B 76 (2007) 165202.
[22] F. Herklotz, E.V. Lavrov, J. Weber, Physica B 404 (2004) 4349.